

Article

Developing Water-Quality Model for Jingpo Lake Based on EFDC

Zihan Qin ^{1,2,3,4}, Zhengwei He ^{1,2,*}, Guozheng Wu ⁵, Gula Tang ^{3,5} and Qian Wang ³

¹ State Key Laboratory of Geohazard Prevention and Geoenvironment Protection, Chengdu University of Technology, Chengdu 610059, China

² College of Earth Sciences, Chengdu University of Technology, Chengdu 610059, China

³ School of Geographical Sciences, China West Normal University, Nanchong 637009, China

⁴ Sichuan Provincial Engineering Laboratory of Monitoring and Control for Soil Erosion in Dry Valleys, China West Normal University, Nanchong 637009, China

⁵ Beijing International Science and Technology Innovation Co., Ltd., Beijing 100070, China

* Correspondence: hzw@cdut.edu.cn; Tel.: +86-028-84078705

Abstract: Water-quality model simulation is the key to understanding hydrological processes and water-quality dynamic(s). In this study, Jingpo Lake, which is the most typical lake in the northern cold region of China, was selected as the research object. A numerical simulation model for transporting and diffusing the chemical oxygen demand (COD_{Mn}) and ammonia nitrogen (NH₃N) with ice-covered and open-water periods was constructed and calibrated using the Environmental Fluid Dynamics Code (EFDC). Parameters such as the bottom roughness, ice roughness, diffusion coefficient, horizontal momentum diffusivity, molecular eddy viscosity, molecular diffusivity, buoyancy influence coefficient, COD_{Mn} decay rate and NH₃N decay rate were validated. The research findings show that there were differences in the hydrodynamic water-quality changing process during the ice-covered and open-water periods, as well as for the seasonal ice-covered waterbody. The key parameter decay rates of the COD_{Mn} and NH₃N in the ice-covered periods were lower than those in the open-water periods due to the water-temperature decline. The R² of the COD_{Mn} and NH₃N reached 90.71% and 79.79%, respectively. Thus, it may be concluded that the EFDC model could well reflect changes in the water level of Jingpo Lake, as well as the transport and diffusion of the COD_{Mn} and NH₃N in Jingpo Lake.

Keywords: cold region; hydrodynamic; water quality; model; numerical simulation



Citation: Qin, Z.; He, Z.; Wu, G.; Tang, G.; Wang, Q. Developing Water-Quality Model for Jingpo Lake Based on EFDC. *Water* **2022**, *14*, 2596. <https://doi.org/10.3390/w14172596>

Academic Editor: Arthur Mynett

Received: 18 July 2022

Accepted: 17 August 2022

Published: 23 August 2022

Publisher's Note: MDPI stays neutral with regard to jurisdictional claims in published maps and institutional affiliations.



Copyright: © 2022 by the authors. Licensee MDPI, Basel, Switzerland. This article is an open access article distributed under the terms and conditions of the Creative Commons Attribution (CC BY) license (<https://creativecommons.org/licenses/by/4.0/>).

1. Introduction

Frozen surface water is a common natural phenomenon at high latitudes. The barring and obstruction of ice covers not only change the water-current structure and the mixing characteristics of the waterbody, but also the transport and diffusion characteristics of the water pollutants [1]. If the river flow is small during ice-covered periods, then the dilution of pollutants will be weakened for two reasons. Firstly, excessively low water temperatures can mitigate the biochemical degradation of water microorganisms on pollutants and lower the self-cleaning capacity of water. Secondly, reaeration is affected by ice covers on the surface, causing the dissolved-oxygen (DO) concentration to decline. Therefore, pollutant transport and diffusion during ice-covered periods is quite different from that during open-water periods [2]. The current research on frozen water has mainly concentrated on the hydrodynamic process [3–5], water temperature [6–8] and the evolution of ice covers [9–11]; there has been little research on the transport and diffusion of pollutants in water. Terry et al. [12], Lima Neto et al. [13] and Obertegger et al. [14] researched the change rule of DO on ice-covered rivers or lakes separately. Arifin et al. [15] simulated the thermal behavior in Lake Ontario using the EFDC and modified EFDC model, and they successfully replicated the thermal-bar evolution. Lin et al. [16] simulated bottom resuspension events in Lake Erie using a coupled three-dimensional hydrodynamic and water-quality model.

Oveysi et al. [17] set up a three-dimensional numerical model of Lake Erie for a winter season using a coupled hydrodynamic and water-quality model (ELCOM-CAEDYM), and validated against observations. The model was successful in predicting the average lake surface temperature. Wang et al. [1] established a (COD) water-quality model for river channels during ice-covered periods to analyze the transport and diffusion law of the COD. Wang et al. [2] researched the COD reduction in rivers during ice-covered periods and constructed a river COD water-quality model. Tang et al. [18] established a numerical simulation model of the river water quality in cold regions of North China with the EFDC model, and they also studied the transport process of the COD and NH_3N in the river channel during open-water periods and ice-covered periods. Su et al. [19] modeled the changing processes of the water temperature and COD concentration during both open-water and ice-covered periods for a seasonally ice-covered reservoir in the cold regions of northern China. Hosseini et al. [20] established a sensitivity analysis framework for the water-quality modeling and monitoring of rivers in cold regions using the Water Quality Analysis Program (WASP7); moreover, the study revealed that the parameter sensitivities differ between ice-covered and open-water periods. Julie A. Terry et al. [21] constructed a sediment-oxygen-demand (SOD) model of Buffalo Pound Lake in Canada using the CE-QUAL-W2 water-quality numerical model to simulate the change law of the SOD during ice-covered and open-water periods; furthermore, the relationship between the SOD and chlorophyll-a (Chla) concentrations was discussed. Meanwhile, Terry et al. [22] also simulated the change processes of the DO, Chla, orthophosphate (PO_4), nitrate/nitrite (NO_3), ammonia (NH_4), water temperature and ice thickness in Buffalo Pound Lake during ice-covered and open-water periods, with unsatisfactory results. The simulation accuracy of all the indexes, except for the water temperature and ice thickness, was low. There are few studies that focus on simulating the transport and diffusion of pollutants in waterbodies during ice-covered periods. There are many challenges ahead, most of which stem from insufficient data to fully parametrize the model during calibration [22]. Nevertheless, a numerical model is still an effective means and research direction for analyzing the law of change in water pollutants during ice-covered periods.

Numerical model tools are widely used in water-quantity and -quality management due to their advantages in comparative efficiency, the visualization of spatial information and applications in data-scarce areas [23]. Scholars have also developed many hydrodynamic water-quality-model tools in the past few decades, including CE-QUAL-W2 [24], QUAL2K [25], MIKE 21 [26], DELFT3D [27], WASP [28], EFDC [29], FVCOM [30], etc., which have been widely applied in rivers, lakes, reservoirs, wetlands, river mouths, bays and oceans, but few application cases have been based on seasonal ice-covered lakes. Therefore, a typical lake, named Jingpo Lake, in the cold region of northern China was selected in this paper as a research object to study the water quality of the lake during ice-covered and open-water periods with the Environmental Fluid Dynamics Code (EFDC), and to reveal the transport of pollutants in the lake in the cold region of northern China. As the COD_{Mn} and NH_3N are the main pollutants in Jingpo Lake, they were chosen as the simulation indexes in this study to construct a new water-quality model for the lake.

The EFDC model, developed by John M. Hamrick at the Virginia Institute of Marine Science, is representative of hydrodynamic and water-quality models. It is a three-dimensional mathematical water-quality model that simulates flow fields, temperature, sediment, dye, the water quality and other factors at different spatial and temporal scales. The model includes modules for dynamics (water depth, 3D currents and mixing), dye-dispersion simulation, water temperature, salinity, near-field plume simulation and particle-drifting simulation. It can also be used to simulate the concentration changes of 21 water-quality indicators, such as the COD, DO, ammonia nitrogen, total nitrogen, total phosphorus, algae, etc. [31]. The EFDC has become one of the recommended models of the US EPA, and it has been widely used across the globe. For example, Wu et al. [32] applied the EFDC in Daoxiang Lake for chlorophyll-a simulation and algal-bloom prediction. Ji et al. [33] simulated the dry and wet grid of a shallow-water estuarine in the Morro Bay area, Cal-

ifornia, based on the EFDC hydrodynamic model. Li et al. [34] constructed a water-age and thermal-structure model for Lake Mead under changing water levels using the EFDC model. Gong et al. [35] used the EFDC to investigate the transport timescale of river-borne sediment in the tidal York River Estuary. Mansoor et al. [36] described the sampled spatial and temporal variability of metals in the Don River, and they developed a modeling strategy to describe the flood metal-transport dynamics using the EFDC. The purpose of this paper is to understand the transport and diffusion behavior of pollutants in a seasonally frozen lake in the cold region of northern China using the EFDC model.

2. Study Area

Jingpo Lake is a lake located in the northeast of China, which lies between a northern latitude of $43^{\circ}45'5.91''$ – $44^{\circ}3'30.50''$ and an eastern longitude of $128^{\circ}46'4.12''$ – $129^{\circ}2'32.03''$ (Figure 1). Jingpo Lake is a typical channel lake; the length of the lake from south to north is about 45 km, and the widest distance between east and west is only 6 km. The area is 95 km^2 , and the storage capacity is 1.63 billion m^3 , with a maximum water depth of 62 m. The lake was created about 10,000 years ago when volcanic eruptions in the region blocked the flow of the Mudanjiang River. A dam was built at the blocked site in 1938 for electricity generation, flood control, agricultural irrigation, the municipal water supply and tourism. The length of the dam is 2633 m. This lake is famous for its craggy limestone cliffs and turquoise-colored waters containing 40 types of fish and freshwater coral. In September 2006, Jingpo Lake joined the Global Geopark Network at the second International Geoparks Conference in Belfast, Northern Ireland. It is a territory with outstanding geological as well as archaeological, ecological and cultural value, and considerable local efforts are being made to preserve and enhance the heritage.

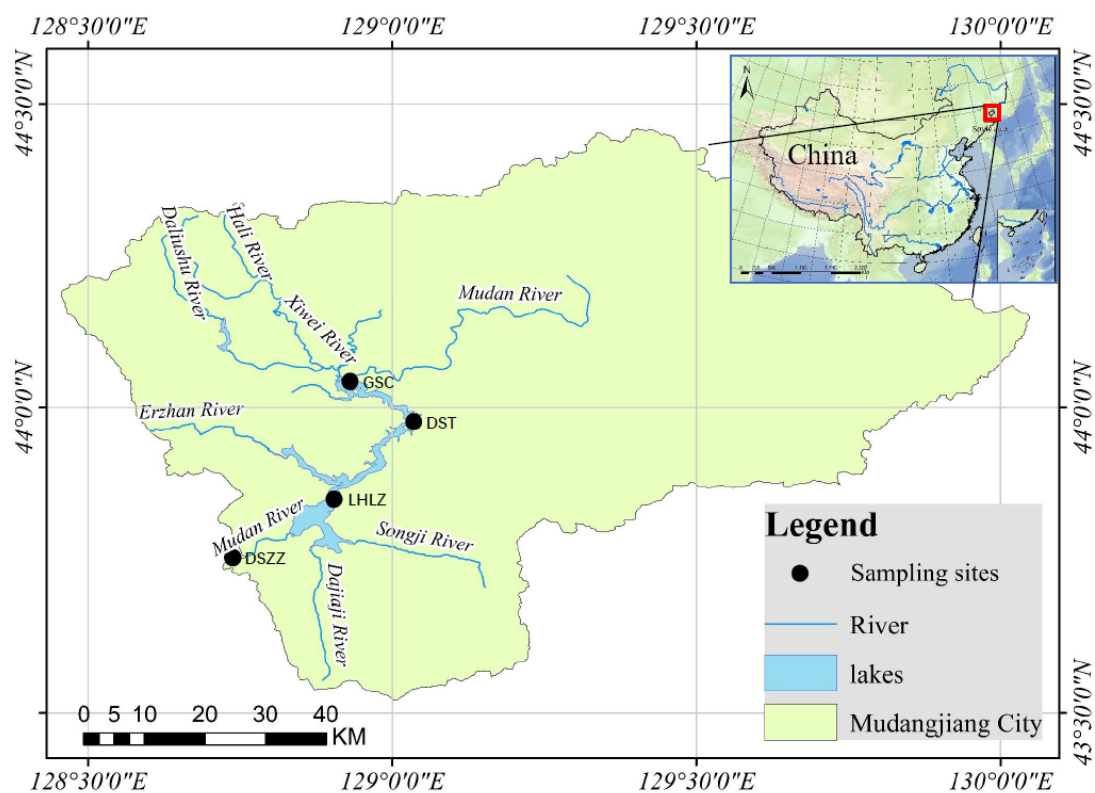


Figure 1. Schematic diagram for Jingpo Lake.

The mean annual precipitation in the Jingpo Lake basin was 647 mm during 1980–2010. The precipitation from June to September accounts for more than 70% of this annual precipitation. The mean annual reservoir inflow of water is 3.02 billion m^3 . The maximum and minimum annual inflows are 5.51 billion m^3 and 730 million m^3 , respectively.

The lake inflow from June to September accounts for 70% of the annual inflow. The lake is frozen in late November and melted in mid-April. The mean thickness of the ice layer is 0.83 m, with the maximum up to 1.04 m. The change characteristics of the water level in Jingpo Lake are presented as follows: The highest water level occurs from August to September, while the lowest level occurs from March to April. The mean annual water level, highest water level and lowest water level are 347.95 m, 354.43 m and 339.17 m, respectively, for multiple years.

The main inflow of Jingpo Lake is the trunk stream Mudan River, with the tributaries Erzhan River and Songyi River (Figure 1). The outlet of the lake is located at the dam in the northeast. Four water-quality sampling sites were established at the inlet, center and outlet of the lake: DSZZ, LHLZ, DST and GSC (Figure 1).

3. Model Construction

3.1. Principle of the Model

The hydrodynamic equations in the EFDC model are based on a three-dimensional incompressible graded-density turbulence-boundary-layer equation set, including the momentum equation, continuity equation and material-transport equation. The Boussinesq assumption [37] is often adopted to facilitate the processing of the buoyancy lift terms caused by density contrast.

In the abovementioned equation set, second-order accuracy finite difference is adopted in the solution. Staggered grid scatter is adopted horizontally [38]. Second-order accuracy finite difference in a three-time-level scheme is adopted in the time integration. The solution is divided into the internal mode and external mode (i.e., free surface gravity waves and shear stresses are solved using splitting methods) [39]. Semi-implicit difference schemes are adopted in the solution in the external mode. The two-dimensional water-level elevation is calculated simultaneously. In this mode, preconditioning is conducted in the conjugate gradient method before solution [40]. The solution method allows for a large-scale time-step calculation. The time step is only constrained by the explicit central difference stability criterion, or the high-order windward advection scheme used for the nonlinear accelerations [41]. An implicit difference scheme with the consideration of vertical diffusion is adopted in the solution in the internal model [42,43].

3.2. Grid Division, Initial Conditions and Boundary Conditions Setting

3.2.1. Grid Division

The water surface of Jingpo Lake was divided, using a mesh generation tool, into 128 columns and 211 rows of grid matrix. The lake surface covered 4958 cells of planar grid, with a maximum cell area of 85,155 m², and a minimum cell area of 6588 m². Differences in the grid-area size are necessary to better fit the lake boundary. The divided cells are shown in Figure 2. The model adopted a dry–wet grid function (i.e., the quality and quantity of the water would not be simulated when the lake bottom appeared). The bottom elevation of the grids was from the bathymetric survey (Figure 3).

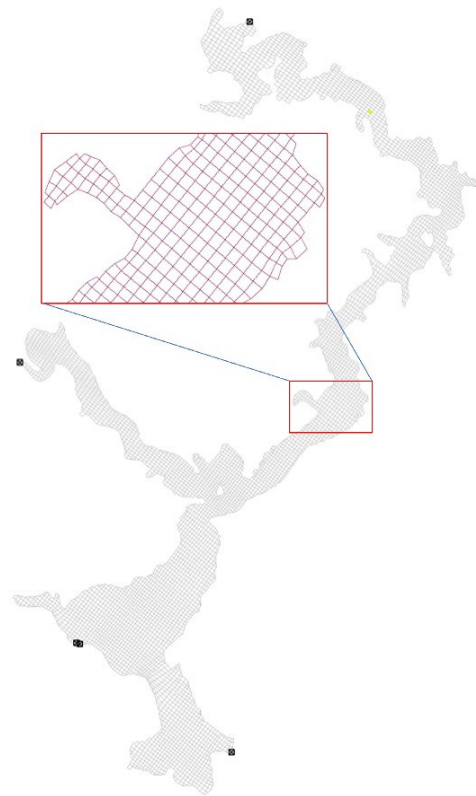


Figure 2. Grid division for Jingpo Lake.

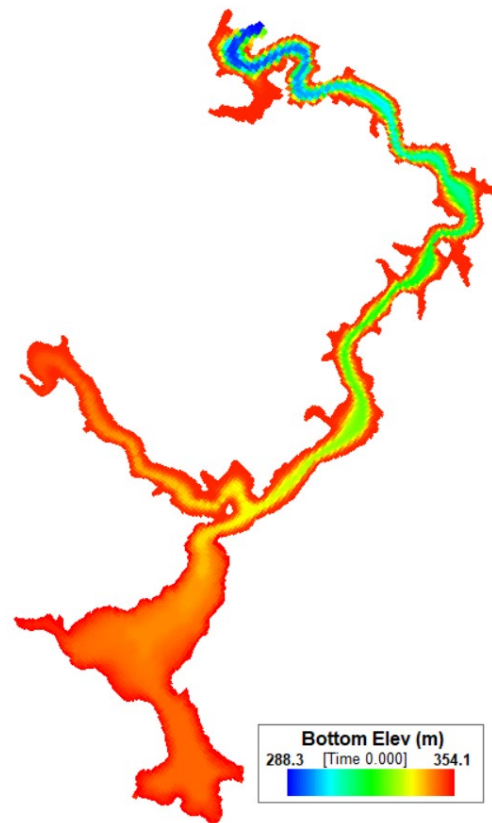


Figure 3. Bottom elevation for Jingpo Lake.

3.2.2. Initial and Boundary Conditions

The initial and boundary conditions are necessities for the EFDC to solve hydrodynamic and water-quality equations. The equations of the numerical model describe the physical, chemical and biological processes within the waterbody. In order to solve these equations numerically, the initial and boundary conditions need to be set. The model was initiated with a stationary condition, according to which the computational domain was assumed to be initially a fixed still-water surface and a zero-flow component. The boundary and external forcing conditions in the computational domain act as driving forces for model simulations, which include inflow–outflow boundaries, inflow temperatures, inflow nutrient loads and atmospheric forces.

The initial condition was the state at 0:00 on 1 January 2017. The initial water level was the measured water level of the lake on 1 January 2017, being at 347.70 m. The initial concentration was obtained by interpolating the measured concentration values of the COD_{Mn} and NH_3N at four water-quality sampling sites (i.e., DSZZ, LHLZ, DST and GSY) on 1 January 2017. According to the measured data, in the simulation, the ice-covered periods ranged from 1 January 2017 to 18 April 2017; from 22 November 2017 to 15 April 2018; from 27 November 2018 to 19 April 2019. The other times are open-water periods.

The inflow boundary conditions included the time series of the inflow of Mudan River, Erzhan River and Songyi River. The lake-inflow-rate data of Mudan River were afforded by the inlet control station of DSZZ. The flow-rate time series of Erzhan River and Songyi River referred to the measured data of Mudan River, and they were calculated via the same multiple scaling method as the basin area. The daily measured discharge flow rate of the dam was adopted as the outflow rate. The daily measured water temperatures of DSZZ were adopted as the inflow temperature boundary condition.

The water-quality boundary conditions contained the time series of the inlet COD_{Mn} and NH_3N concentrations of Mudan River, Erzhan River and Songyi River. The inlet concentration of Mudan River used the measured date of DSZZ Station. During the simulation period, the measured data of DSZZ for the COD_{Mn} and NH_3N concentrations were collected once a month in each year, excluding March, April, November and December because of thin ice sheets during these months.

There are no regular water-quality monitoring data for Erzhan River and Songyi River. Thus, the COD_{Mn} and NH_3N concentrations in the literature [44] are used in this paper and are considered to be constant over the whole simulating period. The concentrations of the COD_{Mn} and NH_3N at the inlets of Erzhan River and Songyi River were 5 mg/L and 0.3 mg/L, respectively.

3.3. Model Parameters and Calibration Method

The model was calibrated with sequential trials by modifying the hydrodynamic and water-quality parameters. The calibrated parameters with definitions and values are listed and explained in Table 1. The model parameters were generally obtained through: (1) direct measurement; (2) estimation from other measured data; (3) literature values; (4) model calibration [45–47]. The criteria for the optimal parameter selection were the mean absolute error (MAE), mean absolute percentage error (MAPE) and coefficient of determination (R^2) between the simulated values and observed values. In this model, the parameters of the ITERM, RP, ZROUGH and ZBRWALL were set as 500, 1.8, 0.035 and 0.002, respectively. The HDRY and HWET were set as 0.05 m and 0.07 m (Table 1), respectively. The AHO, AHD, AVO, ABO and BSC are hydrodynamic parameters, which should be set and verified, while parameters such as the ICEROUGH, RKCOD, RKCODICE, RKNH_3N and RKNH_3NICE , which were significantly distinctive in the open-water period and ice-covered period, should be set and verified separately. It should be noted that the ICEROUGH, reflecting the roughness at the bottom of the ice cover, was set as 0.01 [48].

Table 1. Parameter-calibration results of Jingpo Lake model.

Parameter	Definition	Value	Unit
ITERM	Maximum number of iterations	500	-
RP	Over relaxation parameter	1.8	-
ZROUGH	Bottom roughness	0.035	-
ICEROUGH	Ice roughness	0.01	-
ZBRWALL	Side-wall log-law roughness height	0.002	-
HDRY	Depth at which cell becomes dry	0.05	m
HWET	Depth at which cell becomes wet	0.07	m
AHO	Constant horizontal diffusion	1.0	m ² /s
AHD	Dimensionless horizontal momentum diffusivity	0.05	-
AVO	Background molecular eddy (kinematic) viscosity	1.0×10^{-7}	m ² /s
ABO	Background molecular diffusivity	1.0×10^{-8}	m ² /s
BSC	Buoyancy influence coefficient	1.0	-
RKCOD	COD _{Mn} concentration decay rate in ice-free period	0.0020	1/day
RKCODICE	COD _{Mn} concentration decay rate in ice-covered period	0.0018	1/day
RKNH ₃ N	NH ₃ N concentration decay rate in ice-free period	0.0018	1/day
RKNH ₃ NICE	NH ₃ N concentration decay rate in ice-covered period	0.0015	1/day

4. Results and Discussion

4.1. Hydrodynamics

The values of the AHO, AHD, AVO, ABO and BSC were set as 1.0, 0.05, 1.0×10^{-7} , 1.0×10^{-8} and 1.0, respectively (Table 1). The simulated value and observed value of the water level were compared, as shown in Figures 4 and 7.

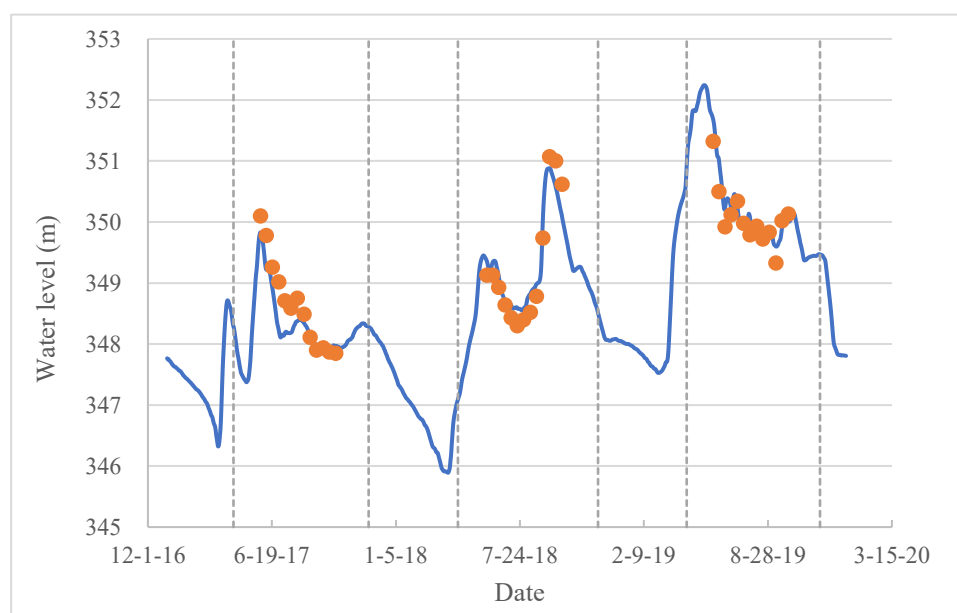


Figure 4. Comparison of the simulation value and measured value of water level in Jingpo Lake. Note: The vertical dotted line in the figure is the boundary between open-water periods and ice-covered periods. The narrow zones represent the ice-covered periods, and the wide zones represent the open-water periods (the same as in Figures 5 and 6).

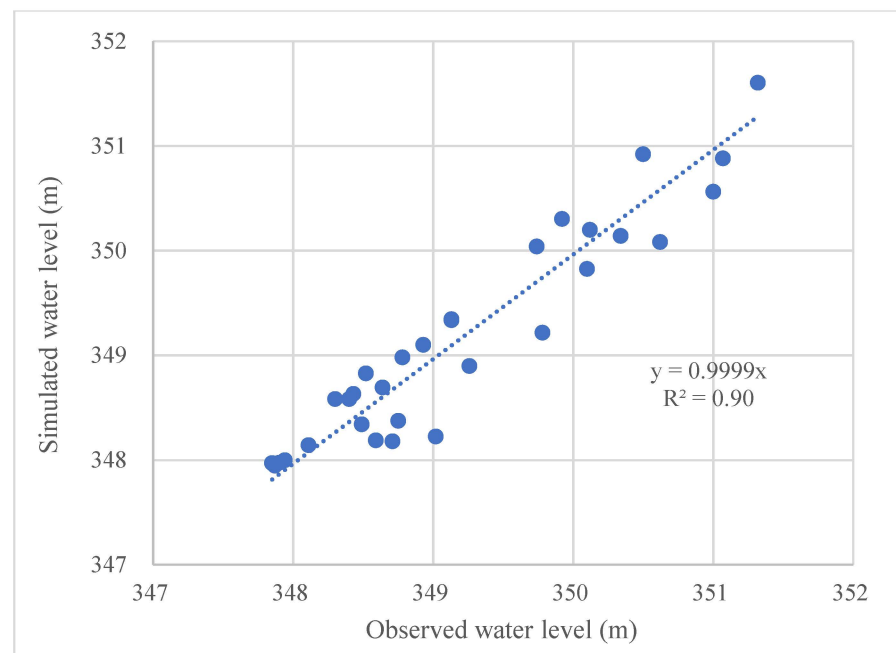


Figure 5. Comparison of the observed and simulated values of COD_{Mn} at: (a) LHLZ sampling site; (b) DST sampling site; (c) GSC sampling site.

The MAE, MAPE and R^2 were used to assess the performance of the model due to its direct interpretability. Figure 4 shows that the maximum error between the observed value and simulated value was 0.79 m, which occurred on 30 June 2017, and the minimum error was 0.05 m, which occurred on 30 June 2018. The calculated MAE, MAPE and R^2 for the water-level errors were 0.27 m, 0.08% and 0.90 (Figure 7), respectively. The statistical analysis results of the water level show that the simulated values were in excellent agreement with the observed values, which provides a satisfactory prerequisite for water-quality simulation.

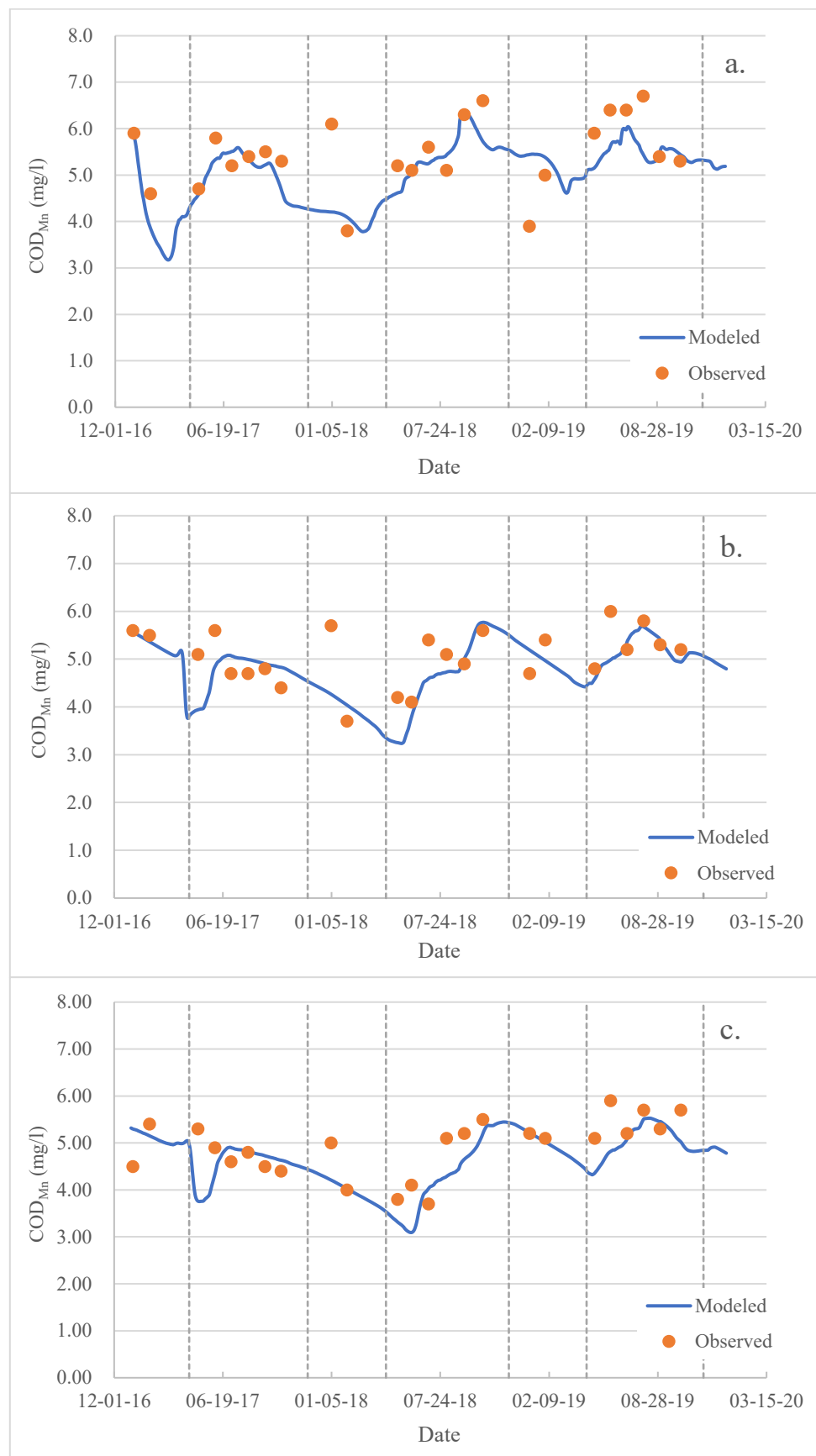


Figure 6. Comparison of the observed and simulated values of NH₃N at: (a) LHLZ sampling site; (b) DST sampling site; (c) GSC sampling site.

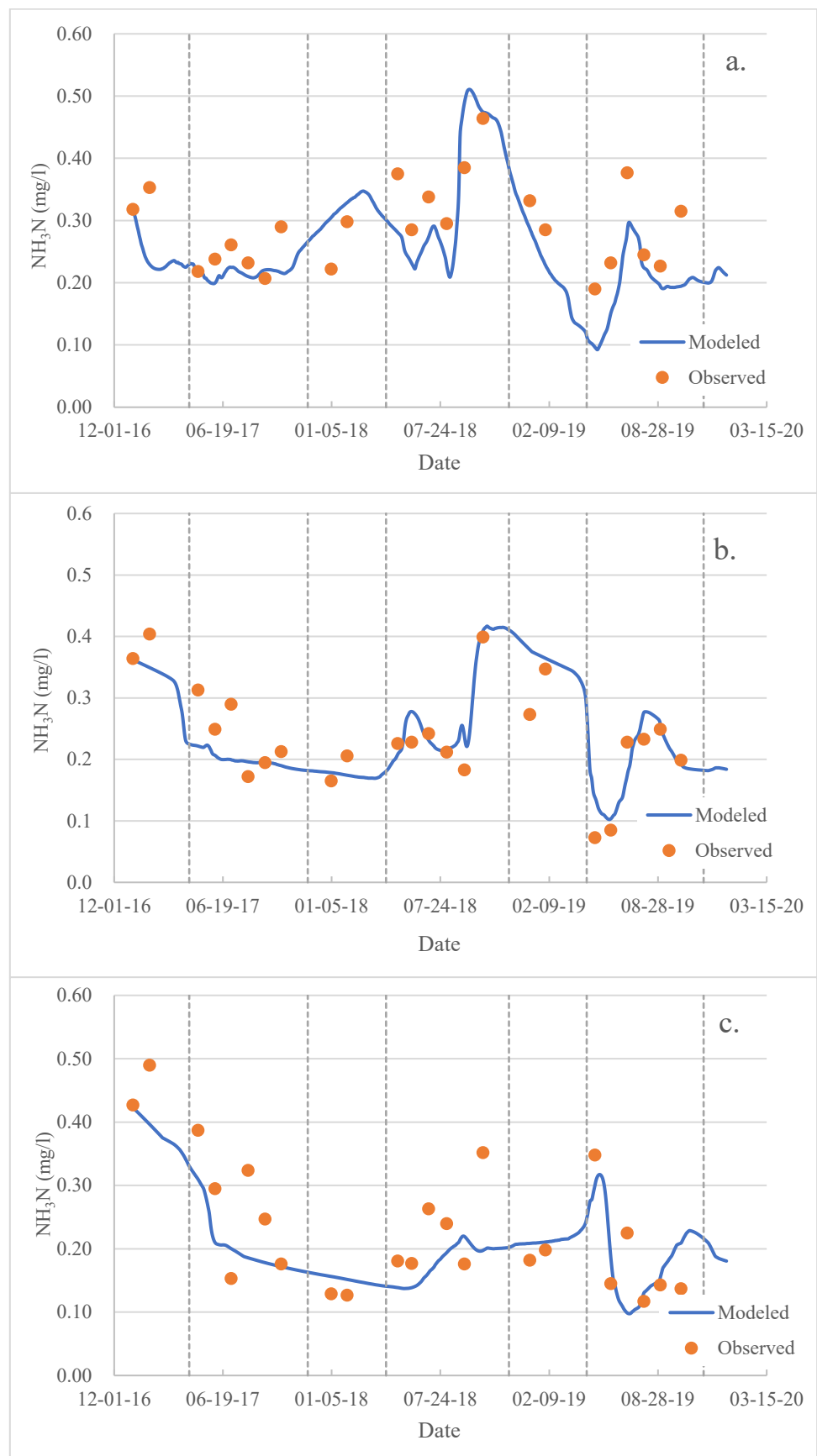


Figure 7. Analysis of the correlation between the simulated values and measured values of water level.

4.2. Water Quality

There were four water-quality sampling sites in this study. Each site has 24 monitoring datasets, of which 6 sampled ice-covered periods and 18 sampled open-water periods. Among them, the water-quality monitoring data of the DSZZ were used as the water-quality boundary condition, which was not involved in the model verification. The water-quality monitoring data obtained from the other three sampling sites (LHLZ, DST and GSC) were utilized for the model verification.

Dynamic simulations of the COD_{Mn} and NH_3N concentrations were conducted through repeat trials, and the key parameter decay rates in the open-water periods and ice-covered periods were calibrated as 0.0020 and 0.0018, and 0.0018 and 0.0015 per day, respectively (Table 1). The statistical analysis results of the COD_{Mn} and NH_3N between the simulated and observed values for each sampling site are listed in Tables 2 and 3. The fitting curves of the simulated and observed values of the COD_{Mn} and NH_3N concentrations for each sampling site are shown in Figures 5 and 6.

Table 2. Statistical results for COD_{Mn} between simulated and observed values in Jingpo Lake model.

Simulation Period	LHLZ			DST			GSC			Total		
	Sample Size	MAE (mg/L)	MAPE (%)	Sample Size	MAE (mg/L)	MAPE (%)	Sample Size	MAE (mg/L)	MAPE (%)	Sample Size	MAE (mg/L)	MAPE (%)
Ice-Covered Period	6	0.82	17.19	6	0.48	9.30	6	0.33	6.79	18	0.54	11.09
Ice-Free Period	18	0.42	7.06	18	0.43	8.52	18	0.52	10.49	54	0.45	8.69
Total Accuracy	24	0.52	9.59	24	0.44	8.71	24	0.47	9.57	72	0.48	9.29 90.71

Table 3. Statistical results for NH_3N between simulated and observed values in Jingpo Lake model.

Simulation Period	LHLZ			DST			GSC			Total		
	Sample Size	MAE (mg/L)	MAPE (%)	Sample Size	MAE (mg/L)	MAPE (%)	Sample Size	MAE (mg/L)	MAPE (%)	Sample Size	MAE (mg/L)	MAPE (%)
Ice-Covered Period	6	0.06	19.39	6	0.04	13.56	6	0.03	13.58		0.04	15.51
Ice-Free Period	18	0.06	19.78	18	0.03	18.21	18	0.06	27.34		0.05	21.78
Total Accuracy	24	0.06	19.68	24	0.03	17.05	24	0.06	23.9		0.05	20.21 79.79

The MAE values and MAPE values of the COD_{Mn} in the ice-covered and open-water periods of the LHLZ station were 0.82 mg/L and 17.19%, and 0.42 mg/L and 7.06%, respectively (Table 2), demonstrating that the simulation errors for the ice-covered period were greater than those for the open-water period. In terms of the DST station, the errors during the ice-covered periods and open-water period were not much different; the MAE value and MAPE value were 0.48 mg/L and 9.30%, respectively, in the ice-covered period, and 0.43 mg/L and 8.52%, respectively, in the open-water period. The errors of the GSC in the open-water period were higher than in the ice-covered period; the MAE value and MAPE value were 0.33 mg/L and 6.79%, respectively, in the ice-covered period, and 0.47 mg/L and 10.49%, respectively, in the open-water period. It can be observed from the whole simulation period that there was no significant difference in the simulation errors of the LHLZ, DST and GSC stations. The MAE values were 0.52 mg/L, 0.44 mg/L and 0.47 mg/L, respectively, while the MAPE values were 9.59%, 8.71% and 9.57%, respectively, all of which are less than 10%. The overall accuracy of the model was 90.71%.

The statistics in Table 3 show that the MAE values of the NH_3N in the ice-covered and open-water periods of the LHLZ station were 0.06 mg/L, while the MAPE values were 19.39% and 19.78%, respectively. Their errors were almost the same. The MAE value and MAPE value of the DST station were 0.04 mg/L and 13.56%, respectively, in the ice-covered periods, and 0.03 mg/L and 18.21%, respectively, in the open-water period. Their errors in the open-water period were higher than in the ice-covered period. The MAE value and MAPE value of the GSC station were 0.03 mg/L and 13.58%, respectively, in the ice-

covered period, and 0.06 mg/L and 27.34%, respectively, in the open-water period. It can be observed from the whole simulation period that the MAE values of the LHLZ, DST and GSC stations were 0.06 mg/L, 0.03 mg/L and 0.06 mg/L, respectively, while their MAPE values were 19.68%, 17.05% and 23.9%, respectively. The overall accuracy of the model was 79.79%. The changing trend of the concentration can be well presented by the simulation results of the COD_{Mn} and NH₃N (Figures 5 and 6).

4.3. Discussion

The water-quality model is an effective method for studying the changing process of pollutants in waterbodies. Constructing a successful hydrodynamic water-quality model, or a model with a high accuracy of simulation, is affected by many factors, such as the measured data of the bottom configuration of the waterbody, hydraulic structures, flow, water levels, sediment, suspended matter, air temperature, water temperature, wind speed, wind direction, rainfall, evaporation as well as the integrity and continuity of the water-quality data to be simulated. In most simulation studies on water quality, it is nearly impossible for all types of observation data to fully satisfy the requirements of the simulation model. Therefore, when constructing these models, some factors that have less influence on the accuracy of the model are often ignored or are set as constant in the course of constructing these models.

In this study, the mean annual precipitation and mean annual potential evaporation of the Jingpo Lake basin were 647 mm and 1023.5 mm [49], respectively. That is to say, the loss was 376.5 mm, which, when converted to water volume, was 35.77 million m³ in the whole lake during a year. In comparison to the mean lake volume of 3.01 billion m³, the effect of rainfall and evaporation could be completely ignored. There tends to be southwesterly winds in the summer and northwesterly winds in the winter in Jingpo Lake, whereas the southwesterly winds dominate for the rest of the year. The mean annual wind speed was 2.6 m/s [44], and it reached a force of 2 on the Beaufort scale [50], which is a light breeze. Under such a circumstance, the wind force has a minor effect on the flow field of Jingpo Lake. Hence, the effects of the wind speed and wind direction were not considered in this study.

Sediment and suspended matter are also important factors that affect the accuracy of the simulation of water quality. Sediment plays an important carrier role in the transport of pollutants [51]. Hu et al. [52] studied the concentration value of the COD_{Mn} under different types of sediment of the Yellow River, and they discovered that the concentration of the COD_{Mn} increases with the increment of the sediment concentration when the Yellow River is turbid, and the measured value of the COD_{Mn} increases with the increment of the sediment concentration when the Yellow River is clear. This indicates that a handful of sediment had minor effects on the change in the concentration of pollutants. The upper reaches of Jingpo Lake, with a high forest cover, offer good conditions for vegetation. The river has a small amount of sediment during the normal and dry seasons, while the river is carried with certain sediment during the flood season, causing it to become turbid [53]. According to the measured data of the sediment concentration, the mean annual sediment concentration of Mudan River is only 0.11 kg/m³, and it is classified as clean water [54]. Thus, the effects of sediment and suspended matter on the water quality could be ignored in this model.

What is more, each year, Jingpo Lake is in the ice-covered period for about 5 months. The thickness of the ice cover varies in the ice-covered period. In theory, the changes in the thickness of ice covers will have different effects on the hydrodynamic process and the process of pollutant transportation, which is called the ice roughness in the index. The ice roughness actually changed with the thickness of the ice cover. However, as there are few research findings on the ice-cover and ice-thickness monitoring data of Jingpo Lake, the ice roughness was set as 0.01 in this study, which refers to the recommended value in the literature [1].

Regarding the seasonal ice-covered waterbody, differences could be found in the changing process of the hydrodynamic water quality during the ice-covered and open-water periods, which were mainly the differences between the ice roughness and decay rate in this model. The hydrodynamic process and diffusion process of the pollutants on the surface water in the ice-covered period were significantly different from those in the open-water period. It should be noted that further study should be conducted on the quantification of the differences between the open-water period and ice-covered period, such as horizontal and vertical changes in the flow fields, changes in water-temperature layering and changes in the mixing process of pollutants in water. Another significant difference between the ice-covered period and open-water period was the difference in the decay rate of the pollutants. The decay rates of the COD_{Mn} and NH_3N in the open-water period in this model were 0.0020 and 0.0018 per day, respectively. When the water temperature in the ice-covered period was decreased, the decay rates also dropped to 0.0018 and 0.0015 per day, respectively.

The uncertainty of the numerical simulation model is affected by many factors, such as measuring errors, data loss and the coarseness of the spatial or temporal data resolution. Although some of the water-quality monitoring data used in this study were obtained from government agencies, these data were usually sampled with a coarse temporal and spatial resolution. Moreover, with only eight instances of monitoring performed in 12 months, the points of water-quality sampling only on the water surface could not present the distribution characteristics of the pollutants in the vertical direction. Continuous sampling at a high frequency will be of great help to improve the accuracy of the modeling simulation. As boundary conditions have a great effect on the simulation model, installing a water-quality automatic monitor to continuously measure the water quality of Jingpo Lake can further promote the accuracy of the model. In addition, it is necessary to measure the frozen process and climate change if the effects of ice covers are to be researched profoundly [55–58].

All in all, although some factors concerning the accuracy of the water-quality model were ignored in this study with the simplified boundary conditions of Erzhan River and Songyi River, the model accuracy of the COD_{Mn} and NH_3N reached 90.71% and 79.79%, respectively. Furthermore, the model could be objectively used to show the transport process of pollutants in Jingpo Lake, and the actual water-quality management of the lake. More importantly, the model could also provide a reference for constructing hydrodynamic water-quality models for lakes and reservoirs of the same type.

5. Conclusions

This study built a new hydrodynamic water-quality numerical model on the basis of the EFDC for Jingpo Lake, located in the northeast of China. The changing processes of the COD_{Mn} and NH_3N concentrations from 1 January 2017 to 31 December 2019 were analyzed during ice-covered and open-water periods, respectively. Parameters such as the bottom roughness, diffusion coefficient, horizontal momentum diffusivity, molecular eddy viscosity, molecular diffusivity, buoyancy influence coefficient, COD_{Mn} decay rate and NH_3N decay rate were calibrated and validated. The main differences in the model parameters between the ice-covered period and open-water period were found to be the decay rates and roughness. The decay rates of the COD_{Mn} and NH_3N in the ice-covered period were lower than those in the open-water period. In the ice-covered model, both the bottom roughness and ice roughness needed to be considered; in comparison, there was no ice roughness in the open-water period.

The statistical results showed that the MAE (mean absolute error), MAPE (mean absolute percentage error) and R^2 (coefficient of determination) for the water-level errors were 0.27 m, 0.08% and 0.90, respectively. The simulation value of the water level was in perfect agreement with the observed value. The MAE and MAPE in the ice-covered and open-water periods for the COD_{Mn} were 0.54 mg/L and 11.09%, and 0.45 mg/L and 8.69%, respectively. The MAE and MAPE in the ice-covered and open-water periods for the NH_3N were 0.04 mg/L and 15.51%, and 0.05 mg/L and 21.78%, respectively.

The research findings show that there were differences in the hydrodynamic water-quality changing process during the ice-covered and open-water periods, as well as for the seasonal ice-covered waterbody. The main reason of these differences may be the changes of ice-cover and water temperature. The barring and obstruction of ice covers change the transport and diffusion characteristics of the water pollutants. Meanwhile, low water temperatures mitigate the biochemical degradation of water microorganisms on pollutants. In the future, we will use the EFDC or other water-quality models to perform advanced research on the mechanism of the ice-sheet and water-temperature impact on water quality.

Based on the simulation results, the simulation accuracy of the COD_{Mn} and NH₃N reached 90.71% and 79.79%, respectively. Although factors such as rainfall, evaporation, wind force, sediment and suspended matter were ignored in the model, and the boundary conditions for the flow and water quality of Erzhan River and Songyi River were simplified, the hydrodynamic water-quality model constructed in this study could well present the changes in the water level in the lake, and the transport process of the COD_{Mn} and NH₃N in Jingpo Lake. The neglect or simplification of the aforementioned factors are therefore acceptable.

In summary, this work provides useful information for understanding the transport processes of water pollutants in a seasonally ice-covered waterbody. The model can be used to model water-contaminating behavior or to conduct normal water-quality forecasts in water-environment management for lakes, reservoirs or ponds located in cold areas.

Author Contributions: Data curation, Z.Q. and G.T.; methodology, Z.Q., Q.W. and G.W.; writing—original draft preparation, Z.Q.; writing—review and editing, Z.H.; All authors have read and agreed to the published version of the manuscript.

Funding: The research was jointly funded by the Independent Research Project of the State Key Laboratory of Geohazard Prevention and Geoenvironment Protection Independent Research Project (SKLGP2021Z003) and by Natural Science Foundation of Sichuan Province(2022NSFSC1040).

Data Availability Statement: The data presented in this study are available upon request from the corresponding author.

Acknowledgments: The authors are grateful for the help from He Zhengwei in the article writing and revision, and for the help from Wu Guozheng, Tang Gula and Wang Qian in the data processing. They are also grateful for the help from the Beijing International Science and Technology Innovation Co. in the data support, as well as the associate editors and reviewers for their comments.

Conflicts of Interest: The authors declare no conflict of interest.

References

1. Wang, Z.G. Water Quality Characteristics and Simulation Methods of Northern Rivers during Ice-Covered Periods. Ph.D. Thesis, Tsinghua University, Beijing, China, 2013.
2. Wang, X.E.; Dong, D.M.; Zhao, W.J.; Li, J.; Zhang, H.L.; Du, Y.G. Reduction Mode of Organic Pollutants in Rivers during the Icebound Season. *J. JILIN Univ. Sci. Ed.* **2003**, *41*, 392–395.
3. Huttulaa, T.; Pulkkanenb, M.; Arkhipovc, B.; Leppäranta, M.; Solbakov, V.; Shirasawa, K.; Salonen, K. Modelling circulation in an ice-covered lake. *Est. J. Earth Sci.* **2010**, *59*, 298–309. [[CrossRef](#)]
4. Lotsari, E.; Tarsa, T.; Kämäri, M.; Alho, P.; Kasvi, E. Spatial variation of flow characteristics in a subarctic meandering river in ice-covered and open-channel conditions: A 2D hydrodynamic modelling approach. *Earth Surf. Process. Landf.* **2019**, *44*, 1509–1529. [[CrossRef](#)]
5. Shen, H.H. Modelling ocean waves in ice-covered seas. *Appl. Ocean Res.* **2019**, *83*, 30–36. [[CrossRef](#)]
6. Yang, B.; Wells, M.G.; McMeans, B.C.; Dugan, H.A.; Rusak, J.A.; Weyhenmeyer, G.A.; Brentrup, J.A.; Hrycik, A.R.; Laas, A.; Pilla, R.M.; et al. A New Thermal Categorization of Ice-Covered Lakes. *Geophys. Res. Lett.* **2021**, *48*, e2020GL091374. [[CrossRef](#)]
7. Forrest, A.L.; Laval, B.E.; Pieters, R.; Lim, S.S.D. A cyclonic gyre in an ice-covered lake. *Limnol. Oceanogr.* **2013**, *58*, 363–375. [[CrossRef](#)]
8. Kletetschka, G.; Fischer, T.; Mls, J.; Dedecek, P. Temperature fluctuations underneath the ice in Diamond Lake, Hennepin County, Minnesota. *Water Resour. Res.* **2013**, *49*, 3306–3313. [[CrossRef](#)]
9. Yang, F.; Feng, W.Y.; Matti, L.; Yang, Y.; Merkouriadi, I.; Cen, R.; Bai, Y.; Li, C.; Liao, H. Simulation and Seasonal Characteristics of the Intra-Annual Heat Exchange Process in a Shallow Ice-Covered Lake. *Sustainability* **2020**, *12*, 7832. [[CrossRef](#)]

10. Kubat, I.; Sayed, M.; Savage, S.; Carrieres, T. Numerical simulations of ice thickness redistribution in the Gulf of St. Lawrence. *Cold Reg. Sci. Technol.* **2010**, *60*, 15–28. [[CrossRef](#)]
11. Xiao, J.M.; Jin, L.H.; Xie, Y.G.; Huo, Y.D. Study on mechanism of formation and melting of reservoir ice cover in cold area. *J. Hydraul. Eng.* **2004**, *6*, 80–85.
12. Terry, D.P. River-ice ecology. I: Hydrologic, geomorphic, and water-quality aspects. *J. Cold Reg. Eng.* **2001**, *15*, 1–16.
13. Lima Neto, I.E.; Zhu, D.Z.; Rajaratnam, N.; Yu, T.; Spafford, M.; McEachern, P. Dissolved oxygen downstream of an effluent outfall in an ice-covered river: Natural and artificial aeration. *J. Environ. Eng.* **2007**, *133*, 1051–1060. [[CrossRef](#)]
14. Obertegger, U.; Obrador, B.; Flaim, G. Dissolved oxygen dynamics under ice: Three winters of high-frequency data from Lake Tovel, Italy. *Water Resour. Res.* **2017**, *53*, 7234–7246. [[CrossRef](#)]
15. Arifin, R.R.; James, S.C.; Pitts, D.A.; Hamlet, A.F.; Sharma, A.; Fernando, H.J.S. Simulating the thermal behavior in lake Ontario using EFDC. *J. Great Lakes Res.* **2016**, *42*, 511–523. [[CrossRef](#)]
16. Lin, S.; Boegman, L.; Valipour, R.; Bouffard, D.; Ackerman, J.D.; Zhao, Y. Three-dimensional modeling of sediment resuspension in a large shallow lake. *J. Great Lakes Res.* **2021**, *47*, 970–984. [[CrossRef](#)]
17. Oveisy, A.; Rao, Y.R.; Leon, L.F.; Bocaniov, S.A. Three-dimensional winter modeling and the effects of ice cover on hydrodynamics, thermal structure and water quality in Lake Erie. *J. Great Lakes Res.* **2021**, *40*, 19–28. [[CrossRef](#)]
18. Tang, G.L.; Zhu, Y.Q.; Wu, G.Z.; Li, J.; Li, Z.L.; Sun, J.L. Modelling and analysis of hydrodynamics and water quality for rivers in the northern cold region of China. *Int. J. Environ. Res. Public Health* **2016**, *13*, 408. [[CrossRef](#)]
19. Su, W.; Wu, G.Z.; Tang, G.L.; Shi, S.H. Modelling and Analysis of Water Quality for Reservoir in the Northern Cold Region of China. *Fresen. Environ. Bull.* **2021**, *30*, 8602–8612.
20. Hosseini, N.; Chun, K.P.; Wheeler, H.; Lindenschmidt, K.E. Parameter Sensitivity of a Surface Water Quality Model of the Lower South Saskatchewan River—Comparison Between Ice-On and Ice-Off Periods. *Environ. Model. Assess.* **2017**, *22*, 291–307. [[CrossRef](#)]
21. Terry, J.A.; Sadeghian, A.; Lindenschmidt, K.E. Modelling dissolved oxygen/ Sediment oxygen demand under ice in a shallow eutrophic prairie reservoir. *Water* **2017**, *9*, 131. [[CrossRef](#)]
22. Terry, J.A.; Sadeghian, A.; Baulch, H.M.; Chapra, S.C.; Lindenschmidt, K.E. Challenges of modelling water quality in a shallow prairie lake with seasonal ice cover. *Ecol. Model.* **2018**, *384*, 43–52. [[CrossRef](#)]
23. Wang, Y.H.; Jiang, Y.Z.; Liao, W.H.; Gao, P.; Huang, X.M.; Wang, H. 3-D hydro-environmental simulation of Miyun Reservoir, Beijing. *J. Hydro-Environ. Res.* **2014**, *8*, 383–395. [[CrossRef](#)]
24. Cole, T.M.; Wells, S.A. CE-QUAL-W2: A Two-Dimensional, Laterally Averaged, Hydrodynamic and Water Quality Model, Version 4.0. In *Department of Civil and Environmental Engineering*; Portland State University: Portland, OR, USA, 2016.
25. Chapra, S.C.; Pelletier, G.J. *QUAL2K: A Modeling Framework for Simulating River and Stream Water Quality: Documentation and Users Manual*; Tufts University: Medford, MA, USA, 2003.
26. *Mike 21 ECOLab Module, Users Guide and Reference Manual*; Danish Hydraulic Institute: Horsholm, Denmark, 2004.
27. WL/Delft Hydraulics. Technical Reference Manual Delft3D-WAQ[EB/OL]. Available online: <http://www.deltares.nl> (accessed on 24 June 2022).
28. Wool, T.A.; Ambros, R.B.; Martin, J.L.; Comer, E.A.; US Environmental Protection Agency; Environmental Research Laboratory; USACE; Tetra Tech, Inc. *Water Quality Analysis Simulation Program (WASP) Version 6.0: Draft User's Manual*; Environmental Protection Agency: Atlanta, GA, USA, 2001.
29. Park, K.; Kuo, A.Y.; Shen, J.; Hamrick, J.M. A three-dimensional hydrodynamic-eutrophication model (HEM-3D): Description of Water Quality and Sediment Process Submodels. In *Special Report in Applied Marine Science and Ocean Engineering No. 327*; Virginia Institute of Marine Science; College of William & Mary: Gloucester Point, VA, USA, 1995.
30. Chen, C.C.; Beardsley, R.C.; Cowles, G. An unstructured grid, finite-volume coastal ocean model (FVCOM) system. *Oceanography* **2006**, *19*, 78–89. [[CrossRef](#)]
31. Hamrick, J.M.; Wu, T.S. Computational design and optimization of the EFDC/HEM3D surface water hydrodynamic and eutrophication model. In *Next Generation Environmental Models and Computational Methods*; Delich, G., Wheeler, M.F., Eds.; Society for Industrial and Applied Mathematics: Philadelphia, PA, USA, 1997; pp. 143–161.
32. Wu, G.Z.; Xu, Z.X. Prediction of algal blooming using EFDC model: Case study in the Daoxiang Lake. *Ecol. Model.* **2011**, *222*, 1245–1252. [[CrossRef](#)]
33. Ji, Z.G.; Morton, M.R.; Hamrick, J.M. Wetting and drying simulation of estuarine processes. *Estuar. Coast. Shelf Sci.* **2001**, *53*, 683–700. [[CrossRef](#)]
34. Li, Y.P.; Acharya, K.; Chen, D.; Stone, M. Modeling water ages and thermal structure of Lake Mead under changing water levels. *Lake Reserv. Manag.* **2010**, *26*, 258–272. [[CrossRef](#)]
35. Gong, W.Q.; Shen, J. A model diagnostic study of age of river-borne sediment transport in the tidal York River Estuary. *Environ. Fluid Mech.* **2010**, *10*, 177–196. [[CrossRef](#)]
36. Mansoor, S.Z.; Louie, S.; Lima, A.T.; Cappellen, P.V.; MacVicar, B. The Spatial And Temporal Distribution Of Metals In An Urban Stream: A Case Study Of The Don River In Toronto, Canada. *J. Great Lakes Res.* **2018**, *44*, 1314–1326. [[CrossRef](#)]
37. Boussinesq, J. *Theorie Analytique de la Chaleur*; Gauthier-Villars: Paris, France, 1903.
38. Arakawa, A.; Lamb, V.R. Computational design of the basic dynamical processes of the UCLA general circulation model. *Methods Comput. Phys.* **1977**, *17*, 174–265.
39. Madala, R.V.; Piacsek, S.A. A semi-implicit numerical model for Baroclinic Oceans. *J. Comput. Phys.* **1977**, *23*, 167–178. [[CrossRef](#)]

40. Sheng, Y.P.; Butler, H.L. Modeling coastal currents and sediment transport. In Proceedings of the 18th International Conference on Coastal Engineering, ASCE, New York, NY, USA, 14–19 November 1982; pp. 1127–1148.
41. Smolarkiewicz, P.K.; Margolin, L.G. On forward-in-time differencing for fluids: Extension to a curvilinear framework. *Mon. Weather Rev.* **1993**, *121*, 1847–1859. [[CrossRef](#)]
42. Sheng, Y.P. Finite-difference models for hydrodynamics of lakes and shallow seas. In *Physics-Based Modeling of Lakes, Reservoirs, and Impoundments*; Gray, W.G., Ed.; ASCE: New York, NY, USA, 1986; pp. 146–228.
43. Harmick, J.M. *A Three-dimensional Environmental Fluid Dynamics Computer Code: Theoretical and Computational Aspects*; The College of William and Mary; Virginia Institute of Marine Science: Gloucester Point, VA, USA, 1992.
44. The People’s Government of Mudanjiang. Scenarios for Jingpo Lake Water Quality to Regulated Water Quality Standard. Available online: <http://www.mdj.gov.cn/> (accessed on 20 June 2022).
45. Ji, Z.G. *Hydrodynamics and Water Quality: Modeling Rivers, Lakes, and Estuaries*; John Wiley and Sons, Inc.: Hoboken, NJ, USA, 2007; p. 613.
46. Ji, Z.G.; Hu, G.D.; Shen, J.; Wan, Y.S. Three-dimensional modeling of hydrodynamic processes in the st. Lucie estuary. *Estuar. Coast. Shelf Sci.* **2007**, *73*, 188–200. [[CrossRef](#)]
47. Jin, K.; Hamrick, J.H.; Tisdale, T. Application of three-dimensional hydrodynamic model for lake okeechobee. *J. Hydraul. Eng.* **2000**, *126*, 758–771. [[CrossRef](#)]
48. Wei, L.Y. Flow resistance in ice-covered river. *Eng. J. Wuhan Univ.* **2002**, *35*, 1–9, 38.
49. Ji, Z.Y.; Che, Z.H. Analysis of climatic characteristics of Mudanjiang in recent 30 years. *Priv. Sci. Technol.* **2014**, *10*, 221.
50. He, Y.; Li, Y.T. Review of water quality models for sediment-induced pollution. *Water Resour. Prot.* **2004**, *20*, 5–9, 15.
51. Hu, G.H. Simulated research on water quality for such heavy sediment-containing rivers like Yellow River. *J. Saf. Environ.* **2004**, *4*, 45–48.
52. Zheng, D.C.; Cui, G.; Jin, Z.; Li, D.S.; Piao, Z.Z. Hydrological characteristics of the upper reaches of Mudan River. *J. Northeast. China Inst. Water Conserv. Hydroelectr. Power* **2006**, *24*, 37–38.
53. Qu, M.Y.; Li, T. Analysis of River Sediment Supply in Middle and Downstream Section of Mudanjiang River Mainstream. *Heilongjiang Sci. Technol. Water Conserv.* **2013**, *41*, 38–40.
54. Wang, Q.; Qi, J.; Wu, H.; Zeng, Y.; Shui, W.; Zeng, J.; Zhang, X. Freeze-Thaw cycle representation alters response of watershed hydrology to future climate change. *Catena* **2020**, *195*, 104767. [[CrossRef](#)]
55. Wang, Q.; Zeng, J.; Qi, J.; Zhang, X.; Zeng, Y.; Shui, W.; Xu, Z.; Zhang, R.; Wu, X.; Cong, J. A multi-scale daily SPEI dataset for drought characterization at observation stations over mainland China from 1961 to 2018. *Earth Syst. Sci. Data* **2021**, *13*, 331–341. [[CrossRef](#)]
56. Zeng, J.; Zhang, R.; Qu, Y.; Bentod, V.A.; Zhou, T.; Lin, Y.; Wu, X.; Qi, J.; Shui, W.; Wang, Q. Improving the drought monitoring capability of VHI at the global scale via ensemble indices for various vegetation types from 2001 to 2018. *Weather Clim. Extrem.* **2022**, *35*, 100412. [[CrossRef](#)]
57. Zhang, R.; Qi, J.; Leng, S.; Wang, Q. Long-Term Vegetation Phenology Changes and Responses to Preseason Temperature and Precipitation in Northern China. *Remote Sens.* **2022**, *14*, 1396. [[CrossRef](#)]
58. Wang, Q.; Qi, J.; Li, J.; Cole, J.; Waldhoff, S.; Zhang, X. Nitrate loading projection is sensitive to freeze-thaw cycle representation. *Water Res.* **2020**, *186*, 116355. [[CrossRef](#)]